Journal of Research in Health Sciences
ISSN: 2228-7809 | https://jrhsjournal.com

Supporting Dataset for Fault-Gouge K–Ar Dating in the Lower Buller Gorge, New Zealand

Dr. Pierre Dubois[1]*, Dr. Claire Moreau[2]
[1]Department of Internal Medicine, Sorbonne University, Paris, France
[2]Faculty of Medicine, University of Lyon, Lyon, France

Introduction

This supporting information provides a summary of the methods used for fault-slip analysis, figures which shows all of our data in five stereonets, and a table with localities, and listing of the axial data. We also provide a summary of the K-Ar fault-gouge dating method along with a figure of the XRD plots of the grain-size fractions used for K-Ar dating of the fault gouge.

Method for fault-slip analysis

To evaluate the kinematics of faults in the lower Buller gorge, the orientation of primary and secondary fault planes, the trend and plunge of striations, and the sense of relative displacement on these planes have been mapped. In this study a simple graphical method is applied to determine principal strain axes using the program 'Fault Kinematics' written by Rick Allmendinger (Marrett and Allmendinger 1990; Allmendinger et al. 2012). The method graphically constructs the principal incremental shortening and extension axes for a given population of faults. Each pair of axes lies in the movement plane of the fault (a plane perpendicular to the fault plane that contains the unit vector parallel to the direction of accumulated slip and the normal vector to the fault plane). Furthermore, each pair of axes is at an angle of 45° to each of the vectors. To distinguish between the shortening and extension axes it is necessary to have information on the sense of slip, which has been deduced from the orientation of fibers, striae and fractures associated with the fault (Hancock 1985; Petit 1987). Fiber and striae orientations on slickensides from the subsidiary faults in the mapping area are usually simple and consistent, and are readily interpretable with the geometry of the mapped faults at a regional scale.

Marrett and Allmendinger (1990) proposed that the brittle deformation in a faulted region can be directly related to the geometric moment, which may be expressed as the product of the average displacement and the fault surface area. This approach requires weighting the fault-slip data with the displacement and the fault surface area. Once the moment tensors are summed, strain magnitudes can be calculated. However, we have no information about slip magnitudes and fault surface area. Therefore, we can only determine the orientations (eigenvectors) of the principal strain axes. The absolute magnitudes (eigenvalues) cannot be calculated. The eigenvalues reported in Table S1 are normalized and are a proxy of the strain symmetry (see Ring (2008) for fuller description). As such the eigenvalue-derived strain symmetry, i.e. flattening (X and Y are >1, i.e. negative eigenvalues), plane strain (Y=1) and prolate (Z and Y are <1, positive eigenvalues) are briefly reported in the figure caption for the fault-slip plots. Bingham distribution statistics for axial data are used to optimize clusters of

kinematic axes of a fault array (Mardia 1972). The linked Bingham distribution is equivalent to an unweighted moment tensor summation (a moment tensor sum in which all faults are weighted equally).

Outcrop conditions in the lower Buller gorge are poor and weathering of the rocks can be severe. We have attempted to map at least 10 faults in a given outcrop. However, this was not always possible. In the figure caption we describe the fault pattern from each outcrop, the main text describes aspects of the overall pattern in the lower Buller gorge.

Analytical procedures for fault-gouge dating

Fault gouge samples were hand-crushed in an agate mortar, repeatedly washed with Milli-Q water to remove salts, and placed in an ultrasonic bath for ~15 min to disaggregate and deflocculate clay minerals. The suspensions containing illite were centrifuged to separate each sample into different size fractions according to Stoke's Law: 2.0–0.5μm, 0.5–0.2 μm, 0.2–0.1 μm, <0.1 μm. The x-ray diffraction (XRD) analyses were conducted on a Bruker D4 Endeavour (CoKα radiation), operated at 40 kV and 30 mA.

Many previous studies have shown that shallow crustal faults form at diagenetic temperatures below 200°C. Fault gouges from such environments are assumed to consist of (1) detrital or inherited illite/muscovite (2M1) derived from wall rocks and (2) authigenic or in situ illite (1M/Md) precipitated within the brittle fault zone during faulting (van der Pluijm et al. 2001; Duvall et al. 2011). Based on a two-end member mixing model, quantified percentages of each illite polytypes (1M/Md and 2M) in different clay size fractions and their apparent ^{40}Ar–^{39}Ar or K–Ar ages are used to extrapolate the age of the pure authigenic clay (e.g., van der Pluijm et al. 2001; Uysal et al. 2006; Duvall et al. 2011).

Authigenic illite, detrital or inherited muscovite, and high-temperature authigenic illite-muscovite can be distinguished from each other by the type of crystallographic stacking, which is called polytype. The 1M/1Md polytype is diagnostic for the authigenic illite (the 1M polytype has a higher crystallinity than 1Md, the latter of which may also contain smectite; both polytypes are commonly referred together as 1M/1Md illite), whereas the 2M polytype is diagnostic for detrital or inherited muscovite or highly crystalline illite precipitated at higher temperatures (>250°C; Srodon & Eberl 1984). The polytypes are determined and quantified by XRD analyses. Peaks of 3.49 Å, 3.20 Å, 2.99 Å, 2.86 Å, and 2.79 Å are diagnostic to determine the presence of 2M1 detrital muscovite or highly crystalline illite in samples, whereas 3.63 Å and 3.07 Å indicate the presence of 1M illite. The presence of 1Md illite is detected by the presence of the illite hump around the illite 003 diffraction peak (Grathoff & Moore 1996).

Polytype quantification

The polytypes can be determined and quantified by XRD analyses. For polytype analyses, different size fractions (2-0.5 μm, 0.5-0.2 μm, 0.2-0.1 μm and <1.2 μm) of non-oriented random powder from the fault gouge sample were scanned from 16 to 44°2θ (as suggested by Bailey, 1988 and Moore and Reynolds, 1989) in the

step-scanning mode with a step size of 0.05 degrees and a counting time of 30 second per step. Peaks of 3.20 Å, 3.00 Å, 2.86 Å, and 2.80 Å are diagnostic to determine the presence of $2M_1$ inherited muscovite in samples, whereas 3.63 Å and 3.07 Å indicate the presence of 1M illite. Illite polytype quantification was done according to the technique for the End-member Standards Matching (STD, Boles et al., 2018), which is similar to the WILDFIRE technique that uses calculated patterns (Grathoff & Moore, 1996), except that STD uses natural as opposed to synthetic diffractograms as input (see Boles et al. (2018) for more detail). Polytype quantification uncertainty is estimated at about ±5%. The results in Table 1 show that the three size fractions derived from four different fault-gouge size fractions have various 1Md/2M1 ratios, which systematically correlate with grain size.

K-Ar dating – fault gouge

The K–Ar dating (performed at the CSIRO Perth, Australia) was conducted according to standard methods given in detail by Dalrymple & Lanphere (1969). Potassium content was determined by atomic absorption. The error of K determination of standards is better than 2%. The K blank was measured at 0.50ppm. Argon was extracted from the separated mineral fraction by fusing the sample within a vacuum line serviced by an on-line ^{38}Ar spike pipette. The isotopic composition of the spiked Ar was measured with a high sensitivity, on-line, VG3600 mass spectrometer. Two international standards (HD-B1 and LPG) and one airshot were also analysed. The K-Ar age was calculated using ^{40}K abundance and decay constants recommended by Steiger & Jäger (1978). The age uncertainties take into account the errors during sample weighting, $^{38}Ar/^{36}Ar$ and $^{40}Ar/^{38}Ar$ measurements and K analysis. Uncertainties of K-Ar age are 2 sigma.

Calculation of $2M_1$ illite component of and IAA plot

The wildfire modeling (WF), end-member standards matching (STD) and Rietveld whole-pattern matching (BGMN) are standard methods to quantify the component of $2M_1$ illite (Boles et al., 2018, and references therein). The STD is similar to the WF method except that the measured dataset of natural $1M_d$ and $2M_1$ illite polytype standards as opposed to synthetic diffractograms are used as input. The STD technique usually provides lower analytical uncertainties of less than 5% (Boles et al., 2018). Our XRD patterns for the various grain-size fractions of sample PCC17-12 show significantly higher (020) peaks at 4.44Å (23.25° 2θ Co Kα) than the (002) peaks at 4.96Å (20.79° 2θ Co Kα), suggesting that acceptable sample randomness was achieved (Grathoff & Moore, 1996; Haines & van der Pluijm, 2008). Thus, the peak ratio between (020) and (002) of our XRD patterns is similar to the patterns of natural end-member standards from Boles et al. (2018), indicating that the sample we prepared had similar randomness as the natural standards. Hence, we choose the STD method to quantify the $2M_1$ illite component of our sample. Because a Cu Kα source is used in the Boles' XRD analysis, which is different from Co Kα source of our XRD equipment (Bruker D4 Endeavour), we use the formula $\lambda=2d*\sin\theta$ (where λ is the wavelength of the incident X-ray beam, $\lambda_{Cu}=1.54056$, $\lambda_{Co}=1.78897$; d is the distance

between the lattice plane; θ is the incident glancing angle) to transfer the θ angle for Cu Kα source of Boles' STD dataset to θ angle for Co Kα source. Given that our measured patterns have similar clay end-members, we use the STD dataset to match our measured XRD pattern in the mixing spreadsheet using the lowest variance approach for the specified $2M_1$ peaks (Haines & van der Pluijm, 2008; Boles et al., 2018). In the finest fraction (<0.1 μm) there are many peaks of non-clay minerals (e.g., gypsum, calcite), and we visually matched the specified 2M1 peaks at 3.88Å and 3.2Å in the mixing spreadsheet. Based on an assessment of the analytical error by Boles et al. (2018), we use a ±3% error for the amount of $2M_1$ illite in this study.

PPC17-12, 2-0.5µm

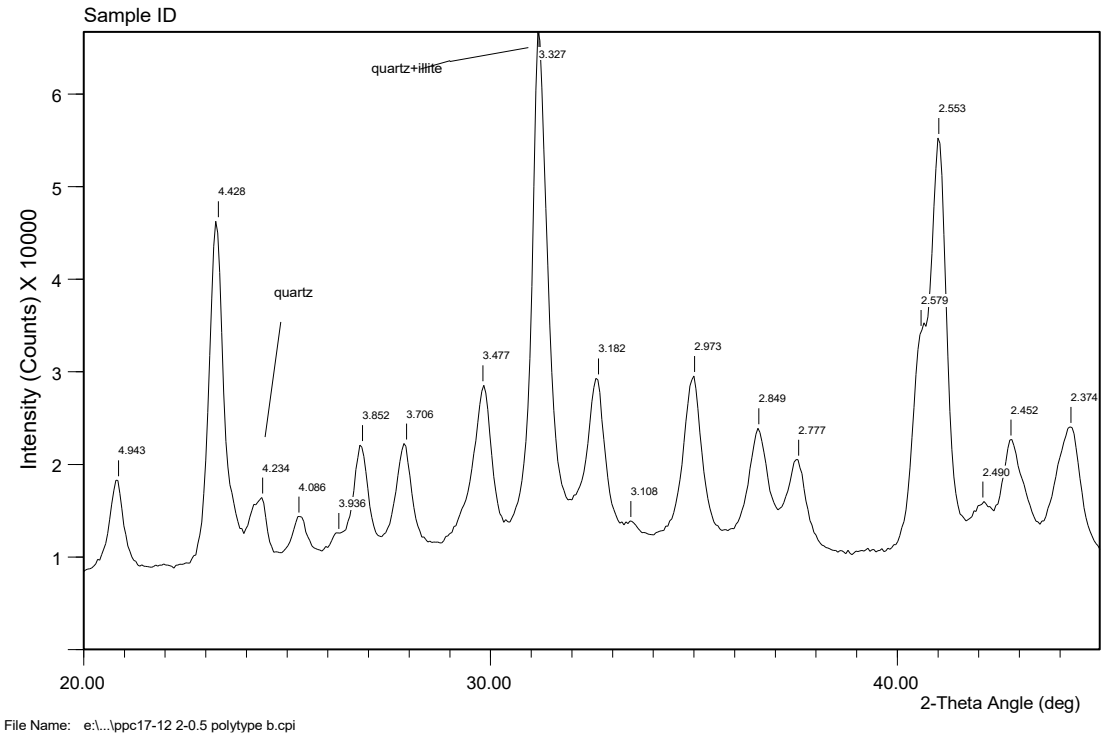

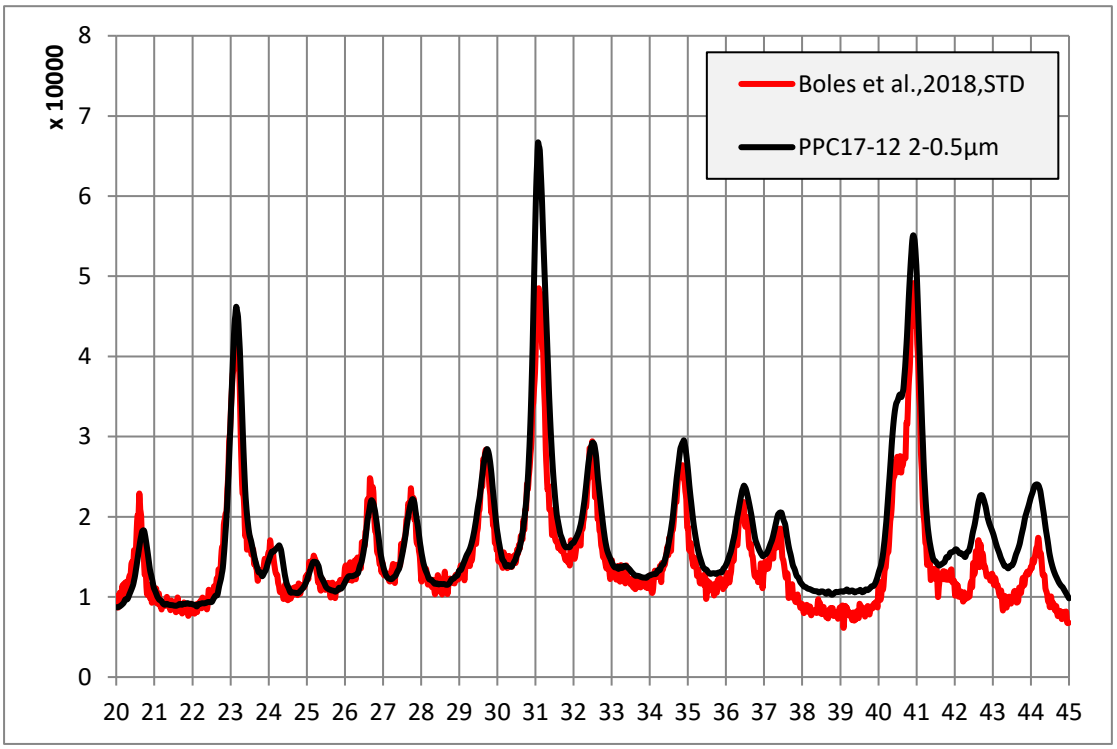

Sample PPC17-12, 2-0.5µm: 94.8% $2M_1$ and 5.2% 1Md illite

PPC17-12, 0.5-0.2µm

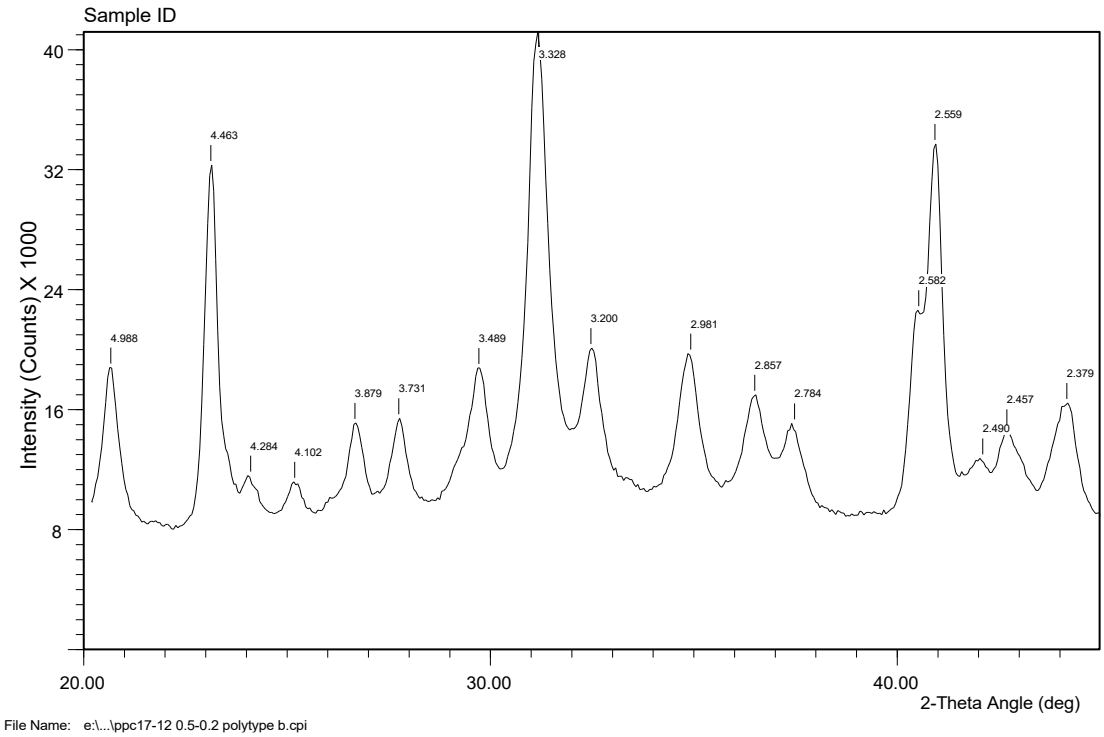

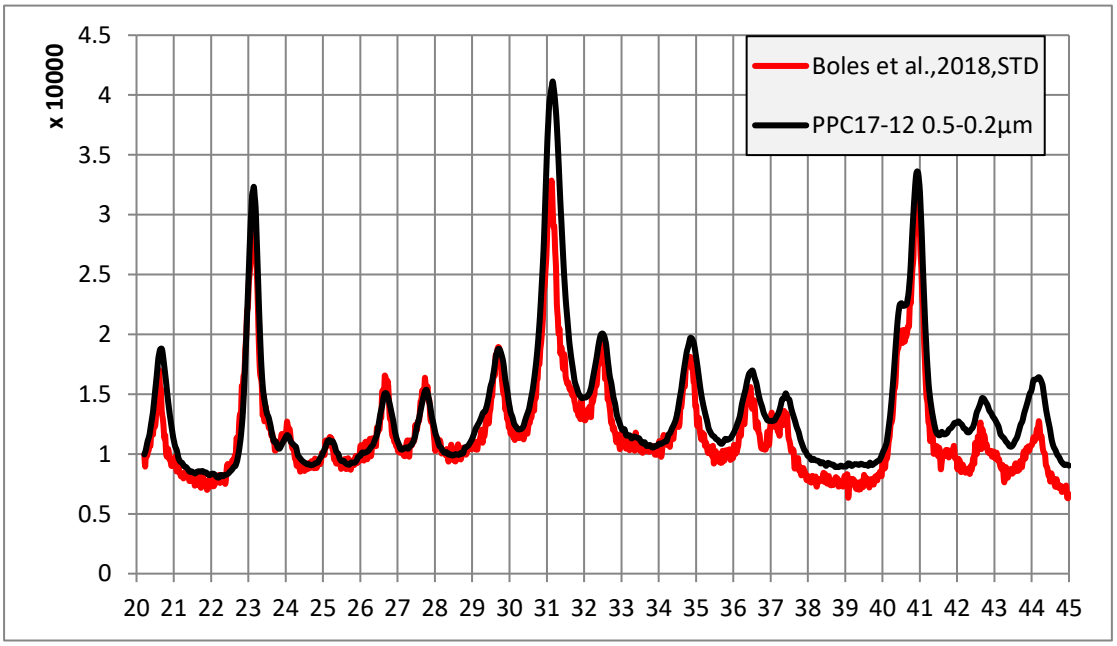

Sample PPC17-12, 0.5-0.2µm: 75.5% $2M_1$ and 24.5% 1Md illite

PPC17-12, 0.2-0.1µm

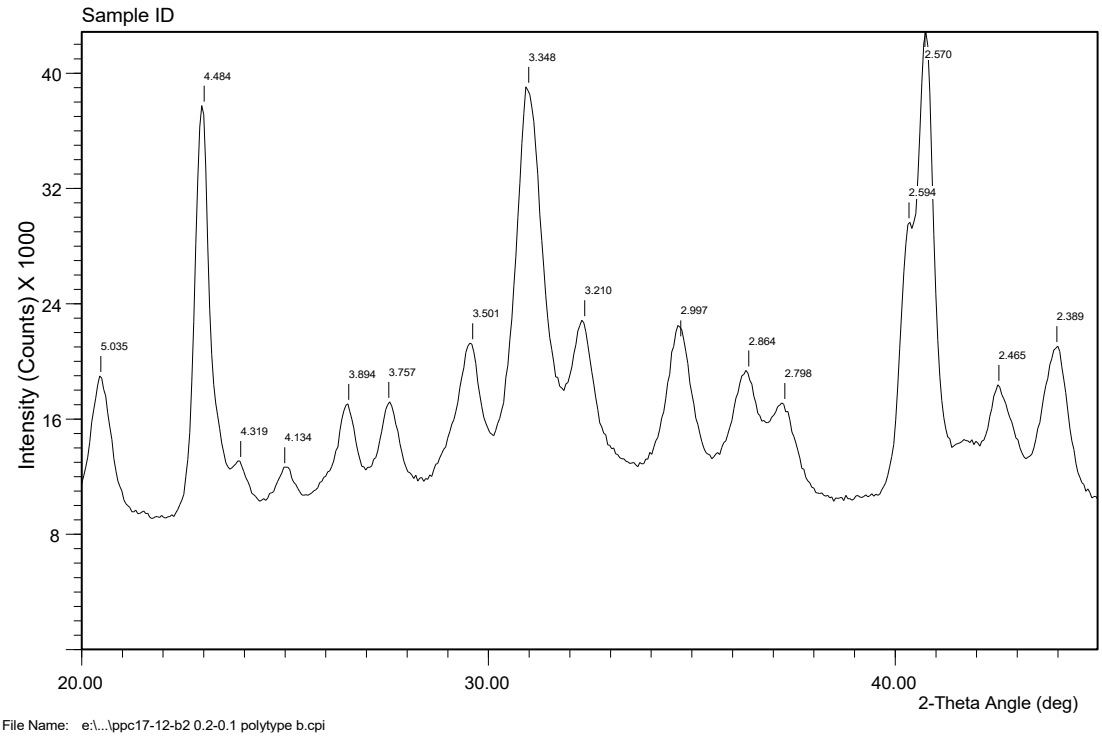

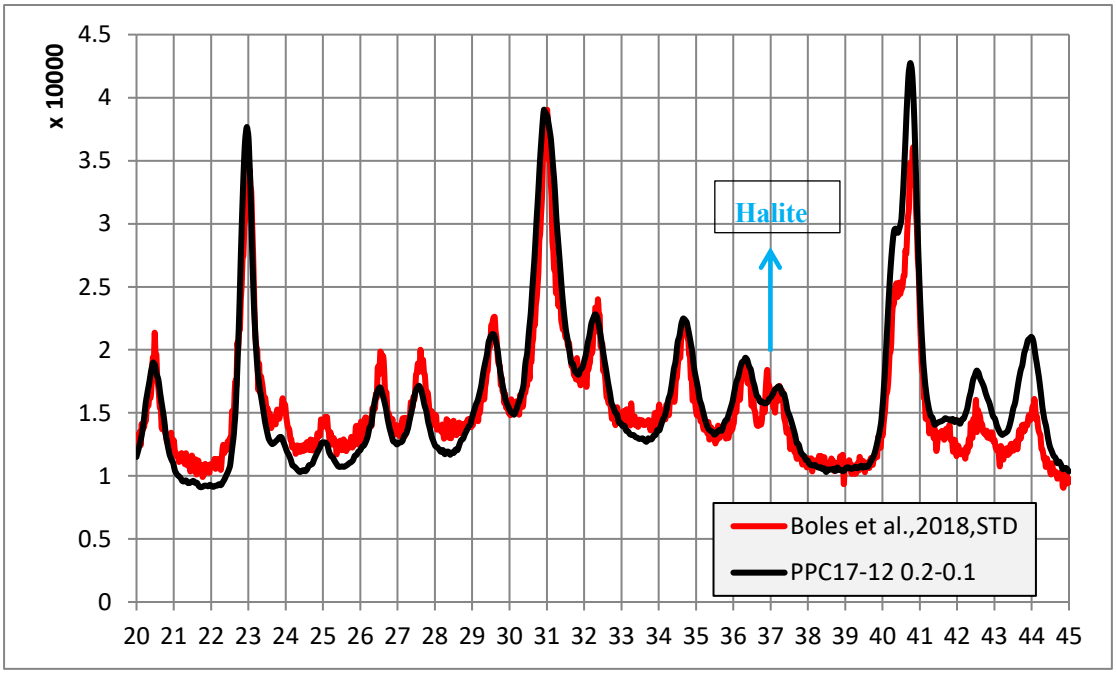

Sample PPC17-12, 0.2-0.1µm: 66.3% $2M_1$ and 33.7% 1Md illite
Note: there is a "halite" peak in the STD Data of Boles et al., 2018

PPC17-12, <0.1µm

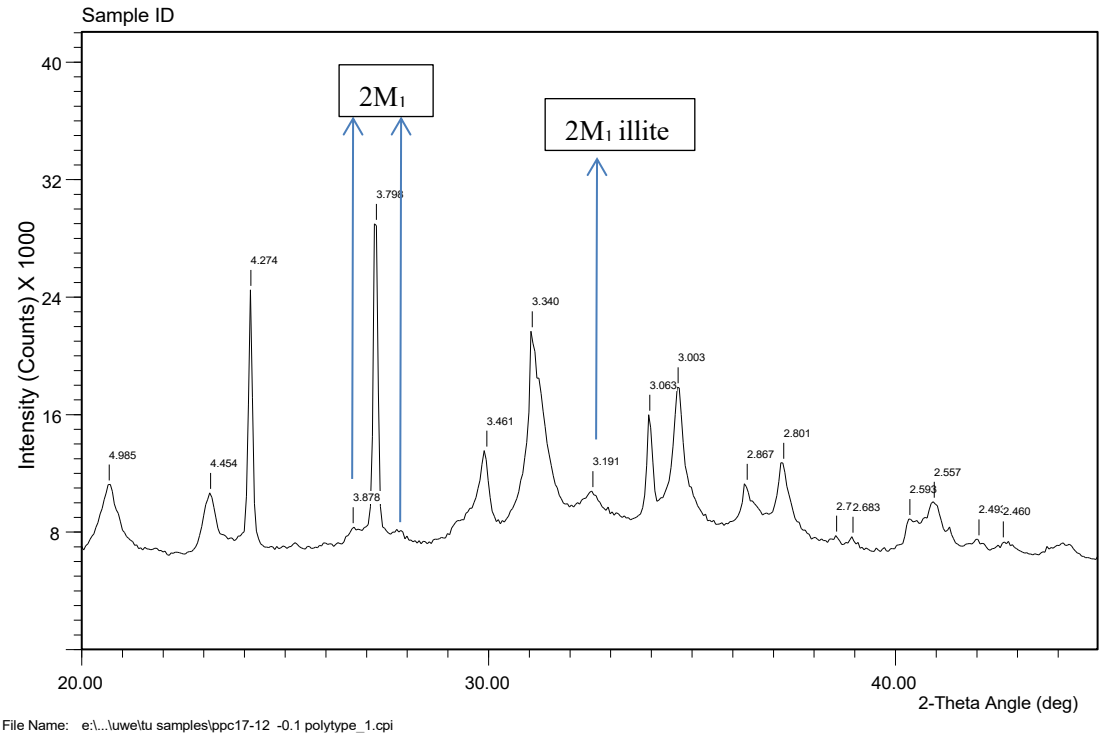

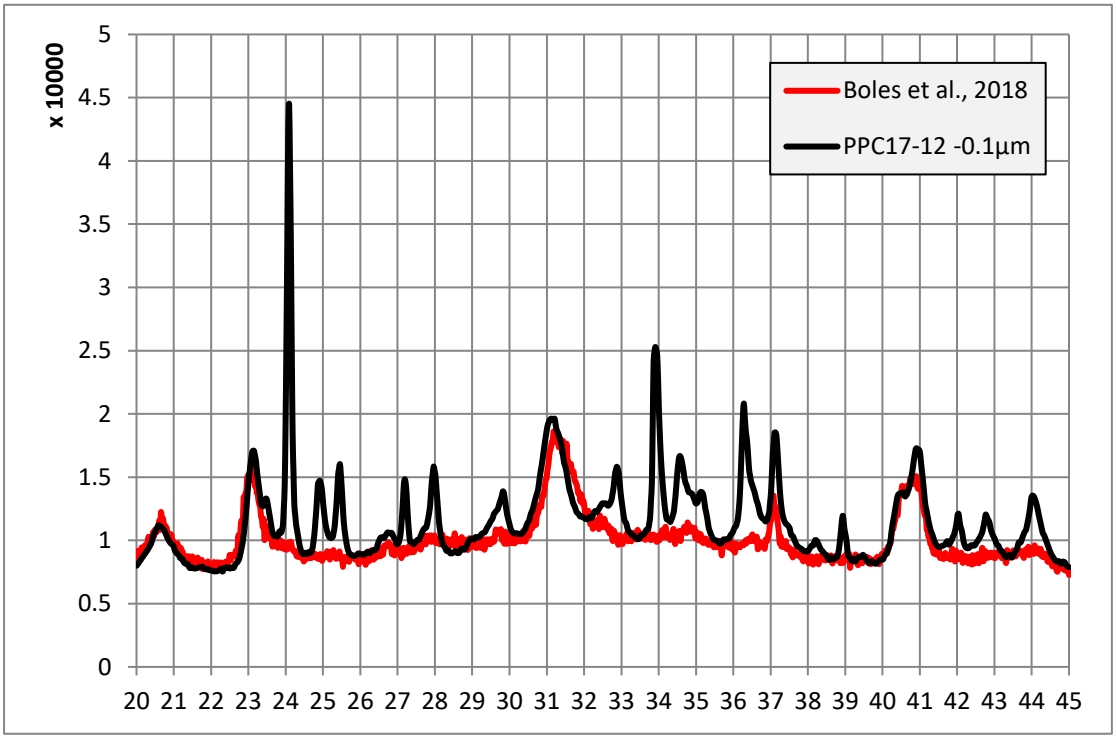

Sample PPC17-12, <0.1µm: 20% $2M_1$ and 80% 1Md illite

Fig. S1. Representative XRD patterns (diagrams on top) and calculated percentage of 2M1 and 1M/1Md illite for grain-size fractions 2-0.5µm, 0.5-0.2µm, 0.2-0.1µm, <0.1µm (diagrams at bottom); numbers above XRD peaks refer to spacing of diffraction angle (d) in Å, while the scale along the y axis shows intensity (counts),

and the one along x axis gives corresponding diffraction angles. STD = End-member Standards Matching (Boles et al. 2019).

Table S1. Table showing K-Ar ages of various grain-size fractions of sample PCC17-12.

Sample	Size fraction	$2M_1$ illite	Error	Age (Ma)	2.5%Error	$e^{\lambda t}-1$	2.5%Error
PPC17-12	2-0.5	94.8	3	98.1	2.4525	0.055882415	0.00136
PPC17-12	0.5-0.2	75.5	3	88.7	2.2175	0.050395132	0.00123
PPC17-12	0.2-0.1	66.3	3	80.5	2.0125	0.045631647	0.001116
PPC17-12	-0.1	20	3	48.5	1.2125	0.027248173	0.000672

References:

Allmendinger, R.W., N.C. Cardozo, and D. Fisher (2012), Structural Geology Algorithms: Vectors & Tensors, pp. 289, Cambridge Univ. Press, Cambridge, U. K.

Bailey, S.W., 1988. X-ray diffraction identification of the polytypes of mica, serpentine, and chlorite. Clay Clay Miner. 36, 193–213.

Boles A., Schleicher A.M., Solum J., Pluijm B.V., 2018. Quantitative X-Ray Powder Diffraction and the Illite Polytype Analysis Method for Direct Fault Rock Dating: A Comparison of Analytical Techniques. Clays and Clay Minerals 66: 220-232.

Boles A., van der Pluijm B., Mulch A., Mutlu H., Uysal I.T. and Warr, L. (2015) Hydrogen and 40Ar/39Ar isotope evidence for multiple and protracted paleofluid flow events within the long-lived North Anatolian Keirogen (Turkey). Geochem. Geophy. Geosy. 16, 1975-1987.

Dalrymple G.B. and Lanphere, M.A. (1969) Potassium-argon dating. W.H. Freeman, San Francisco, 258 p.

Duvall, A.R., Clark, M.K., van der Pluijm, B.A., Li, C., 2011. Direct dating of Eocene reverse faulting in northeastern Tibet using Ar-dating of fault clays and low-temperature thermochronometry. Earth Planet. Sci. Lett. 304, 520–526.

Grathoff, G.H., Moore, D.M., 1996. Illite polytype quantification usingWildfire© calculated X-ray diffraction patterns. Clay Clay Miner. 44, 835–842.

Hancock, P.L. (1985), Brittle microtectonics: Principles and practice, J. Struct. Geol., 7, 437–457.

Mardia, K.V. (1972), Statistics of Directional Data, Academic Press, London.

Marrett, R., and R.W. Allmendinger (1990), Kinematic analysis of fault-slip data, J. Struct. Geol., 12, 973–986.

Moore, D.M., Reynolds, R.C., 1989. X-ray Diffraction and the Identification and Analysis of Clay Minerals. Oxford University Press, Oxford.

Petit, J.-P. (1987), Criteria for the sense of movement on fault surfaces in brittle rocks, J. Struct. Geol., 9, 597–608.

Ring, U. (2008), The tectonic evolution of the Franciscan Subduction Complex: Implications for the exhumation of high-pressure rocks in subduction-related

accretionary wedges, Geol. Soc. Am. Spec. Pap., 445, 1–61, doi:10.1130/2008.2445.

Samson, S.D., Alexander, E.C.J., 1987. Calibration of the interlaboratory 40Ar/39Ar dating standard, MMhb-1. Chem. Geol.: Isot. Geosci. Sect. 66, 27–34.

Steiger R.H. and Jäger E. (1977) Subcommission on geochronology: convention on the use of decay constants in geochronology and cosmochronology. Earth. Planet. Sci. Lett. 36, 359–362.

Uysal I. T., Mutlu M, Altunel A., Karabacak V. and Golding S. D. (2006) Clay mineralogical and isotopic (K–Ar, dO-18, dD) constraints on the evolution of the North Anatolian fault zone, Turkey. Earth. Planet. Sci. Lett. 243, 181–194.

van der Pluijm, B.A., Hall, C.M., Vrolijk, P.J., Pevear, D.R., Covey, M.C., 2001. The dating of shallow faults in the Earth's crust. Nature 412:172–175. http://dx.doi.org/10.1038/35084053.